Sparse Appearance Learning Based Automatic Coronary Sinus Segmentation in CTA

Shiyang Lu[1,3,⋆], Xiaojie Huang[2,3], Zhiyong Wang[1], and Yefeng Zheng[3]

[1] School of Information Technologies, The University of Sydney, Sydney, Australia
[2] Department of Electrical Engineering, Yale University, New Haven, CT
[3] Imaging and Computer Vision, Siemens Corporation, Corporate Technology, Princeton, NJ
yefeng.zheng@siemens.com

Abstract. Interventional cardiologists are often challenged by a high degree of variability in the coronary venous anatomy during coronary sinus cannulation and left ventricular epicardial lead placement for cardiac resynchronization therapy (CRT), making it important to have a precise and fully-automatic segmentation solution for detecting the coronary sinus. A few approaches have been proposed for automatic segmentation of tubular structures utilizing various vesselness measurements. Although working well on contrasted coronary arteries, these methods fail in segmenting the coronary sinus that has almost no contrast in computed tomography angiography (CTA) data, making it difficult to distinguish from surrounding tissues. In this work we propose a multiscale sparse appearance learning based method for estimating vesselness towards automatically extracting the centerlines. Instead of modeling the subtle discrimination at the low-level intensity, we leverage the flexibility of sparse representation to model the inherent spatial coherence of vessel/background appearance and derive a vesselness measurement. After centerline extraction, the coronary sinus lumen is segmented using a learning based boundary detector and Markov random field (MRF) based optimal surface extraction. Quantitative evaluation on a large cardiac CTA dataset (consisting of 204 3D volumes) demonstrates the superior accuracy of the proposed method in both centerline extraction and lumen segmentation, compared to the state-of-the-art.

1 Introduction

Coronary sinus cannulation is a challenging task in cardiac resynchronization therapy (CRT) for novice interventional cardiologists and low-volume operators. Failure to implant left ventricular lead occurs in up to 12% of the procedures as revealed by large clinical trials [1]. This is often due to inability to cannulate the coronary sinus or unfavorable venous anatomy resulting in the inability to find a stable lead position. Therefore, precisely localizing the coronary sinus becomes an urgent demand and would help interventional cardiologists to utilize prior knowledge of coronary venous anatomy for both the selection of patients suitable for CRT and guidance of lead implantation.

⋆ Shiyang Lu and Xiaojie Huang contributed to this work while they were interns at Siemens Corporation, Corporate Technology. They contributed equally to this work.

P. Golland et al. (Eds.): MICCAI 2014, Part I, LNCS 8673, pp. 779–787, 2014.

Several segmentation methods have been proposed to facilitate the identification and localization of coronary venous anatomy from 3D whole-heart acquisitions in computed tomography angiography (CTA) or cardiac magnetic resonance (CMR). In [2], the heart segmentation is achieved automatically but the coronary venous anatomy has to be manually segmented by clinical experts. Sometimes, a few seed points have to be specified by a user to perform a semi-automatic segmentation of the coronary sinus [3,4]. In [5], a 3D cardiac model is applied to extract cardiac chambers and great vessels, including the proximal segment of the coronary sinus. However, the middle and distal segments of the coronary sinus have to be segmented manually. To the best of our knowledge, there is only one study [6] that addresses the fully automatic segmentation of the coronary sinus, which uses the segmented chambers to guide the extraction of coronary sinus.

Quite a few approaches have been proposed for automatic segmentation of coronary arteries in CTA data utilizing various vesselness measurements [7], which potentially can be adapted to segment the coronary sinus. However, most coronary artery segmentation methods are data-driven using no or little high-level prior knowledge, thereby lacking robustness under severe stenosis or low contrast. Recently, Zheng *et al.* [8] present a model-driven approach to predict the initial centerline of a major coronary artery. The initial centerline is further refined using a machine learning based vesselness measurement, which relies on the low-level image intensity features (e.g., it relies on the fact that a coronary artery is brighter than surrounding tissues in CTA). Although this method has achieved excellent robustness on extracting centerlines of coronary arteries (which are contrasted in CTA), it does not work well on coronary sinus because, unlike coronary arteries, the coronary sinus has very weak or no contrast at all in CTA. This presents a big challenge in distinguishing the coronary sinus from surrounding tissues. The problem is further complicated by the large intensity variations inside/outside the coronary sinus.

In this work, rather than modeling the weak discrimination at the low-level intensity, we exploit the flexibility of sparse representation to model the spatial coherence of local appearance inside and outside the coronary sinus. We propose a multiscale sparse appearance learning based approach to estimating a vesselness, which measures the probability of a voxel being at the center of the coronary sinus. Sparse learning has previously been shown to be effective in exploiting spatial coherence in several applications [9]. Here, we employ a multiscale sparse representation model of the local appearance of vessels and background tissues with two series of appearance dictionaries. The appearance dictionaries discriminate image patterns by reconstructing them in the process of sparse learning. We derive an appearance discriminant from the residues as the vesselness measurement score and incorporate the discriminant into a model-driven centerline extraction procedure [8]. After centerline extraction, the original CTA volume is resampled along the extracted centerline for the subsequent boundary detection. The optimal lumen surface is computed by correlating the boundary probabilities with a convex Markov random field (MRF) based graph optimization approach. Experiments on 204 CTA datasets demonstrate that the proposed approach clearly outperforms the state-of-the-art, leading to superior accuracy in both centerline extraction and lumen segmentation.

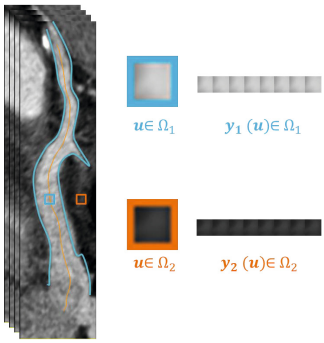

Fig. 1. Construction of appearance vectors for voxels inside (Ω_i^1) and outside (Ω_i^2) of the coronary sinus

2 Coronary Sinus Centerline Extraction

Model-Driven Centerline Extraction. Given an input volume, the heart chambers are segmented using the method presented in [10], and they are then used to predict the initial centerline of the coronary sinus. Afterward, a dynamic programming based optimization is applied to refine the initial centerline path. The initial centerline is represented as a set of evenly sampled points P_i, for $i = 0, 1, \ldots, n-1$. For each point P_i, 41×41 candidate positions P_i^j are uniformly sampled on a plane perpendicular to the centerline path at P_i. The candidates P_i^j are sampled on a regular grid of $20 \times 20\ mm^2$ (with grid spacing of $0.5\ mm$) centered at P_i. We then solve the following shortest path computation problem [8] to select the best position for each point P_i,

$$\bar{P}_0^{J(0)}, \bar{P}_1^{J(1)}, \ldots, \bar{P}_{n-1}^{J(n-1)} = argmin_{P_i^{J(i)}} \sum_{i-0}^{n-1} C(P_i^{J(i)}) + \omega \sum_{i-0}^{n-2} ||P_i^{J(i)} - P_{i+1}^{J(i+1)}||. \quad (1)$$

Here, the first term is the negative of vesselness, penalizing voxels not inside the coronary sinus. The second term is the total length of the path by summing the Euclidean distance between two neighboring points on the path. Free parameter ω, which is used to balance the two terms, is heuristically tuned on a few datasets and then fixed throughout the experiments. In [8], a vesselness measuring the likelihood of a voxel being at the vessel center is learned and estimated via low-level intensity features [11]. To overcome the limitations of this vesselness, in this work, we use a multiscale sparse learning based approach to estimate the likelihood.

Multiscale Sparse Learning for Vesselness Estimation. In cardiac CT images, vessels and background tissues present different appearance in terms of local image patterns. Let Ω denote the 3D image domain. We describe the multiscale local appearance at a voxel $\mathbf{u} \in \Omega$ with a series of appearance vectors $\mathbf{y}^s(\mathbf{u}) \in \mathbb{R}^n$ at different appearance scales $s = 1, \ldots, S$. $\mathbf{y}^s(\mathbf{u})$ is constructed by concatenating orderly the voxels within a block centered at $\mathbf{u}$, as illustrated in Fig. 1. In the following, to simplify the notation, we drop superscript s in $\mathbf{y}^s$ if it does not cause a confusion. Under a sparse

model, an appearance vector $\mathbf{y} \in \mathbb{R}^n$ can be represented as a sparse linear combination of the atoms from an appearance dictionary $\mathbf{D} \in \mathbb{R}^{n \times K}$, $K > n$, which encodes the typical patterns of a corresponding appearance class. Different classes of local appearance are modeled with different appearance dictionaries. Learning an overcomplete dictionary $\mathbf{D} \in \mathbb{R}^{n \times K}$ from a training set $\mathbf{Y} = [\mathbf{y}_1, \ldots, \mathbf{y}_M]$ of M appearances is addressed by minimizing the following reconstruction residual error,

$$\min_{\mathbf{D},\mathbf{X}} ||\mathbf{Y} - \mathbf{D}\mathbf{X}||_2^2, \; s.t., ||\mathbf{X}||_0 \leq T, \tag{2}$$

where $\mathbf{X} = [\mathbf{x}_1, \ldots, \mathbf{x}_K]$ represent the sparse representation of $\mathbf{Y}$ and T is a sparsity factor. We employ the K-SVD algorithm [12] to solve the dictionary learning problem.

For extracting the coronary sinus centerline, we need to discriminate the vessel and the background tissues. Let Ω^1 (the coronary sinus) and Ω^2 (background) denote two local appearance classes, which can be sparsely coded using two appearance dictionaries $\mathbf{D}_1$ and $\mathbf{D}_2$ trained with corresponding samples, respectively [9]. The reconstruction residue of an appearance vector $\mathbf{y}_i$ from class i with respect to dictionary $\mathbf{D}_c$ at the s^{th} scale is defined as

$$\{R(\mathbf{y}_i(\mathbf{u}), \mathbf{D}_c)\}_s = ||\mathbf{y}_i^s(\mathbf{u}) - \{\mathbf{D}_c \hat{\mathbf{x}}_{ic}(\mathbf{u})\}_s||_2, \; \forall i, c \in \{1, 2\}, \tag{3}$$

where $\hat{\mathbf{x}}_{ic}$ is the sparse representation of $\mathbf{y}_i$ obtained via sparse learning (2). Intuitively, an appearance vector from Ω^1 should be reconstructed more accurately using the corresponding dictionary $\mathbf{D}_1$, and vice versa. It is naturally to expect that $\{R(\mathbf{y}_1(\mathbf{u}))\}_s > \{R(\mathbf{y}_2(\mathbf{u}))\}_s$ when $\mathbf{u} \in \Omega^2$, and $\{R(\mathbf{y}_1(\mathbf{u}))\}_s < \{R(\mathbf{y}_2(\mathbf{u}))\}_s$ when $\mathbf{u} \in \Omega^1$. We utilize this local appearance discrimination to estimate the likelihood of a voxel being at the coronary sinus center. By combining the multiscale discriminative information, we obtain a vesselness score for each voxel as

$$p(\mathbf{u}) = \sum_{s=1}^{S} w_s . sgn\{R(\mathbf{y}(\mathbf{u}), \mathbf{D}_2)_s - R(\mathbf{y}(\mathbf{u}), \mathbf{D}_1)_s\}, \tag{4}$$

where w_s is the weighting parameter of the s^{th} appearance scale. This probability indicates the likelihood of voxel $\mathbf{u}$ being at the coronary sinus center, which can be incorporated into the shortest path computation (1) as the cost for a single node.

3 Coronary Sinus Lumen Segmentation

Once the centerline is extracted, the CTA volume is warped and resampled along the centerline path for the subsequent boundary detection. The optimal lumen surface is further computed by correlating the boundary probabilities with a convex Markov random field (MRF) based graph optimization approach [13]. This section describes the necessary steps to segment the coronary sinus lumen surface.

Warping the Volumetric Data. In the first step of lumen segmentation, a warped and re-sampled version of the image volume is generated. The centerline is resampled to a certain resolution (e.g., $0.1\ mm$) to get a homogeneous slice distance. For each

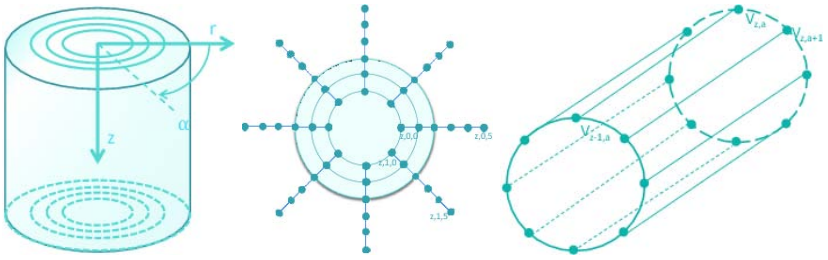

Fig. 2. Coronary sinus lumen segmentation. (a) A cylindrical coordinate space of the warped volume using an extracted centerline; (b) Ray-casting for a discrete sampling; and (c) The tubular MRF graph for lumen surface extraction.

centerline point, an image slice orthogonal to the vessel centerline is extracted where the image is interpolated with bi-linear interpolation at positions between voxels. As illustrated in Fig 2a, the height in the warped volume is expressed by the coordinate z, whereas the angle $\alpha \in [0, 2\pi)$ and the radial distance $r \in \mathbb{R} \geq 0$ uniquely define a point in the other two dimensions, as depicted in Fig. 2a.

Detecting Lumen Boundary. For each slice, R points along each of the T rays are generated. By this way, $T \times Z \times R$ directed candidate boundary points are generated. In this work we utilize the boundary classifier proposed in [10] to calculate boundary probability. Without loss of generality, the predicted boundary probability is a scalar between $[0, 1]$.

Segmenting Lumen Surface. At last, out of all potential boundary candidates we need to select the optimum boundary position as the final segmentation results. The problem is formulated as a first order Markov random field (MRF) with discrete multivariate random variables [13]. A globally optimal configuration for MRFs can be exactly found by calculating the minimal cut in a graph. We thus reduce the surface segmentation task to a network flow problem which can be solved efficiently using the max-flow algorithm.

We firstly re-organize all the boundary candidates in a form such that we can directly incorporate them as the probability distribution of an N_R-label graph-cut problem in the space, $\mathcal{X} = L^V = \{0 \dots N_R - 1\}^{\{0 \dots N_S - 1\} \times \{0 \dots N_A - 1\}}$, where the probabilities of the candidates along with N_R-configurations of ray length are denoted as label assignments $L = \{0 \dots N_R - 1\}$ for every slice N_S and every ray N_A. The corresponding candidates are denoted as the set of vertices V in MRF notation. Thus, a vertex $v_{z,a} \in V$ of the MRF graph represents one element in the problem domain as z is attached to the corresponding slice and a to the ray angle (see Fig. 2c). A network graph $\hat{G} = (\hat{V}, \hat{E})$ can be constructed with the dimensionality of $N_R \times N_S \times N_A$.

After the graph construction, the max-flow-min-cut algorithm proposed by Boykov and Kolmogorov [14] is utilized to estimate the lumen surface. The minimal "s-t" cut bi-partitions the network graph $\hat{G}$ into two groups S and T along the set of labels L such that each vertex $v_{z,a,i} \in V$ is assigned a unique label $i \in \{0, \dots, N_R - 1\}$. The lumen surface can then be defined as a set of contours corresponding to the cross-sections.

Table 1. Comparison of the coronary sinus centerline extraction accuracy of the proposed sparse learning based method and previous vesselness using low-level intensity features [8] on 204 CTA datasets

Methods / Error (mm)	Mean	Std	Median	Min	Max	80^{th} Percentile
Vesselness Using Low-Level Intensity [8]	3.00	1.26	2.84	0.98	9.57	3.82
Proposed Sparse Coding Method	1.52	0.89	1.29	0.50	8.68	1.92

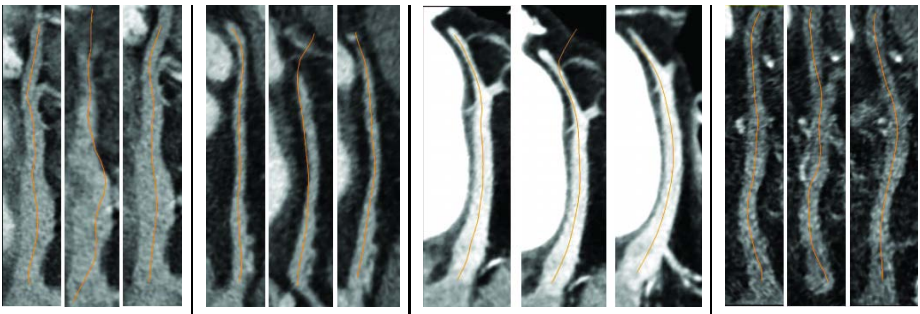

Fig. 3. Automatically extracted coronary sinus centerlines on four CTA volumes. For each volume, the first column shows the ground truth; the second column shows the centerline extracted using [8]; and the last column shows the centerline extracted using the proposed method.

Each contour is generated by determining the length of the N_A rays, resulting in a set of three-dimensional points that define the contour at a specific cross-section. The third dimension of the contour points is given by the index of the corresponding slice, which is attached to a centerline point. The estimated lumen surface in the warped volume is then transferred back to the original volume space.

4 Experiments

In this section we evaluate the proposed coronary sinus segmentation method on CTA data for both the centerline extraction and lumen segmentation. We collected a total of 204 cardiac CTA volumes and manually annotated coronary sinus centerline and lumen mesh for each volume. In our annotation, the coronary sinus starts from its ostium at the right atrium and ends at the bifurcation to great cardiac vein and left marginal vein. A 10-fold cross-validation is performed to evaluate the segmentation accuracy. We also compare our method with the state-of-the-art coronary artery centerline extraction method [8] re-trained for the coronary sinus.

Centerline Extraction Accuracy. Two different centerline extraction algorithms are used to generate the centerline. Both algorithms are model-driven and the only difference is on the vesselness used for shortest path computation in (1). The first algorithm [8] utilizes the low-level intensity features to train a vesselness measurement [11]

Table 2. Coronary sinus lumen segmentation accuracy on 204 CTA datasets

Methods / Error (mm)	Mean	Std	Median	Min	Max	80^{th} Percentile
Based on Centerlines Extracted Using [8]	2.10	1.14	1.92	0.44	7.54	2.80
Proposed Method	0.99	0.73	0.81	0.24	6.30	1.29

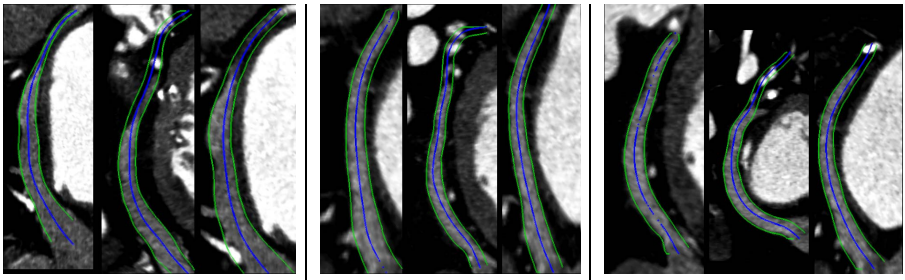

(a) (b) (c)

Fig. 4. Coronary sinus lumen segmentation results on three CTA datasets. For each volume, the first column shows the ground truth; the second column shows the segmentation based on centerlines extracted using [8]; and the last column shows the segmentation based on centerlines obtained with sparse learning.

and the second algorithm uses the proposed sparse learning based vesselness measurement.

Table 1 shows the centerline accuracy on the evaluation set. The proposed method clearly outperforms the low-level intensity based vesselness [11] with mean error of 1.52 mm vs. 3.00 mm. It demonstrates that the multiscale sparse learning based vesselness is more effective in distinguishing the voxels inside and outside the coronary sinus. The maximum centerline error often occurs at the distal end, mainly due to the inaccuracy in determining sinus length. Using a dedicated end-point detector (which is missing in this work) may further improve the centerline accuracy. In Fig. 3, we show centerlines extracted using both approaches on a few representative volumes with various contrast concentration. The proposed method can handle large variation of contrast by the appearance dictionaries learned from a large training set, covering common variations observed in clinical practice. The variations are automatically encoded as different dictionary atoms after training.

Lumen Segmentation Accuracy. In the following experiments, we evaluate the coronary sinus lumen segmentation accuracy. As shown in Table 2, using the proposed method we achieve a mean mesh error of 0.99 mm. Since the lumen segmentation is based on the extracted centerline, the centerline accuracy affects the final lumen segmentation quality. Feeding the lumen segmentation module with the centerlines extracted using [8], we obtain a lumen segmentation error as large as 2.10 mm. Clearly, the multiscale sparse appearance learning based centerline extraction method is a valuable pre-processing step which leads to superior performance in lumen segmentation. Fig. 4 shows a few examples of the coronary sinus lumen segmentation results.

5 Conclusions

In this work we proposed a novel automatic coronary sinus centerline extraction method combining the advantages of the model-driven approach and multiscale sparse appearance learning. The sparse appearance learning based vesselness can effectively distinguish the coronary sinus from background tissues. Based on the extracted centerline, the lumen surface is segmented using a machine learning based boundary detector and MRF based optimal surface extraction. The proposed method has been evaluated on a large dataset of 204 CTA volumes, showing superior accuracy compared to the state-of-the-art.

References

1. Abraham, W.T., Hayes, D.L.: Cardiac resynchronization therapy for heart failure. Circulation 108(21), 2596–2603 (2003)
2. Ma, Y.L., Shetty, A.K., Duckett, S., Etyngier, P., Gijsbers, G., Bullens, R., Schaeffter, T., Razavi, R., Rinaldi, C.A., Rhode, K.S.: An integrated platform for image-guided cardiac resynchronization therapy. Physics in Medicine and Biology 57(10), 2953–2968 (2012)
3. Garcia, M.P., Toumoulin, C., Haigron, P., Velut, J., Garreau, M., Boulmier, D.: Coronary vein tracking from MSCT using a minimum cost path approach. In: IEEE International Conference on Biomedical Imaging, pp. 17–20 (2010)
4. Ordas, S., Oubel, E., Leta, R., Carreras, F., Frangi, A.F.: A statistical shape model of the heart and its application to model-based segmentation. In: Proc. of SPIE Conf. Medical Imaging, vol. 6511 (2007)
5. Duckett, S.G., Ginks, M.R., Knowles, B.R., Ma, Y., Shetty, A., Bostock, J., Cooklin, M., Gill, J.S., Carr-White, G.S., Razavi, R., Schaeffter, T., Rhode, K.S., Rinaldi, C.A.: Advanced image fusion to overlay coronary sinus anatomy with real-time fluoroscopy to facilitate left ventricular lead implantation in CRT. Pacing and Clinical Electrophysiology 34(2), 226–234 (2011)
6. Ecabert, O., Peters, J., Walker, M.J., Ivanc, T., Lorenz, C., von Berg, J., Lessick, J., Vembar, M., Weese, J.: Segmentation of the heart and great vessels in CT images using a model-based adaptation framework. Medical Image Analysis 15(6), 863–876 (2011)
7. Lesage, D., Angelini, E.D., Bloch, I., Funka-Lea, G.: A review of 3D vessel lumen segmentation techniques: Models, features and extraction schemes. Medical Image Analysis 13(6), 819–845 (2009)
8. Zheng, Y., Tek, H., Funka-Lea, G.: Robust and accurate coronary artery centerline extraction in CTA by combining model-driven and data-driven approaches. In: Mori, K., Sakuma, I., Sato, Y., Barillot, C., Navab, N. (eds.) MICCAI 2013, Part III. LNCS, vol. 8151, pp. 74–81. Springer, Heidelberg (2013)
9. Huang, X., Dione, D.P., Compas, C.B., Papademetris, X., Lin, B.A., Sinusas, A.J., Duncan, J.S.: A dynamical appearance model based on multiscale sparse representation: Segmentation of the left ventricle from 4D echocardiography. In: Ayache, N., Delingette, H., Golland, P., Mori, K. (eds.) MICCAI 2012, Part III. LNCS, vol. 7512, pp. 58–65. Springer, Heidelberg (2012)
10. Zheng, Y., Barbu, A., Georgescu, B., Scheuering, M., Comaniciu, D.: Four-chamber heart modeling and automatic segmentation for 3-D cardiac CT volumes using marginal space learning and steerable features. IEEE Transactions on Medical Imaging 27(11), 1668–1681 (2008)

11. Zheng, Y., Loziczonek, M., Georgescu, B., Zhou, S.K., Vega-Higuera, F., Comaniciu, D.: Machine learning based vesselness measurement for coronary artery segmentation in cardiac CT volumes. In: Proc. of SPIE Medical Imaging. vol. 7962, pp. 1–12 (2011)
12. Aharon, M., Elad, M., Bruckstein, A.: K-SVD: An algorithm for designing overcomplete dictionaries for sparse representation. IEEE Transactions on Signal Processing 54(11), 4311–4322 (2006)
13. Ishikawa, H.: Exact optimization for Markov random fields with convex priors. IEEE Trans. Pattern Anal. Machine Intell. 25(10), 1333–1336 (2003)
14. Boykov, Y., Kolmogorov, V.: An experimental comparison of min-cut/max-flow algorithms for energy minimization in vision. IEEE Transactions on Pattern Analysis and Machine Intelligence 26(9), 1124–1137 (2004)